

Reconstructing People, Places, and Cameras

Lea Müller* Hongsuk Choi* Anthony Zhang Brent Yi Jitendra Malik Angjoo Kanazawa
UC Berkeley

{mueller, hongsuk, anthony_zhang1234, brentyi, malik, kanazawa}@berkeley.edu

* equal contribution

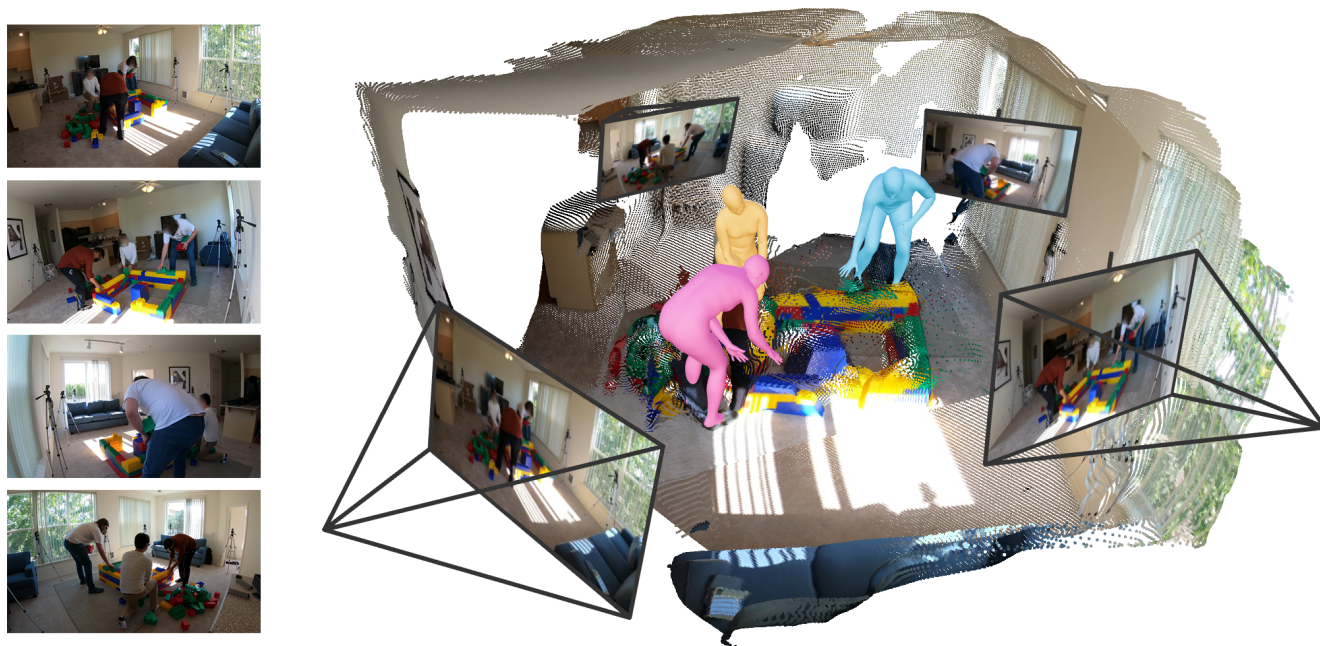


Figure 1. **Humans and Structure from Motion (HSfM)**. We propose a method for the joint reconstruction of humans, scene point clouds, and cameras from an uncalibrated, sparse set of images depicting people. By explicitly incorporating humans into the traditional Structure from Motion (SfM) framework through 2D human keypoint correspondences and leveraging robust initialization from an off-the-shelf model for scene and camera reconstruction, our approach demonstrates that integrating these three elements—people, scenes, and cameras—synergistically improves the reconstruction accuracy of each component. Unlike prior work in SfM and human pose estimation, our method reconstructs metric-scale scene point clouds and camera parameters, informed by human mesh predictions, while situating human meshes in coherent world coordinates consistent with the surrounding environment without any explicit contact constraints.

Abstract

We present “Humans and Structure from Motion” (HSfM), a method for jointly reconstructing multiple human meshes, scene point clouds, and camera parameters in a metric world coordinate system from a sparse set of uncalibrated multi-view images featuring people. Our approach combines data-driven scene reconstruction with the traditional Structure-from-Motion (SfM) framework to achieve more accurate scene reconstruction and camera estimation while simultaneously recovering human meshes. In con-

trast to existing scene reconstruction and SfM methods that lack metric scale information, our method estimates approximate metric scale by leveraging the human statistical model. Furthermore, our method reconstructs multiple human meshes within the same world coordinate system with the scene point cloud, effectively capturing spatial relationships among individuals and their positions in the environment. We initialize the reconstruction of humans, scenes, and cameras using robust foundational models and jointly optimize these elements. This joint optimization synergistically improves the accuracy of each component. We com-

pare our method with existing methods on two challenging benchmarks, *EgoHumans* and *EgoExo4D*, demonstrating significant improvements in human localization accuracy within the world coordinate frame (reducing error from 3.51m to 1.04m in *EgoHumans* and from 2.9m to 0.56m in *EgoExo4D*). Notably, our results show that incorporating human data into the SfM pipeline improves camera pose estimation (e.g., increasing RRA@15 by 20.3% on *EgoHumans*). Additionally, qualitative results show that our approach improves scene reconstruction quality. Our code is available at muelea.github.io/hsfm.

1. Introduction

In recent years, combining deep learning with multi-view geometry has led to significant advances in two key areas: 3D human reconstruction [16, 23] and scene reconstruction [48, 53]. However, progress in these domains has largely evolved independently. Human reconstructions often lack anchoring within their surrounding scenes, while scene reconstructions typically exclude people and fail to recover metric scale. In this paper, we propose a unified framework that bridges these two elements.

We introduce *Humans and Structure from Motion (HSfM)*, a new method that enables the joint reconstruction of multiple human meshes, scene point clouds, and camera parameters within the same metric world coordinate system as shown in Figure 1. From a sparse set of uncalibrated multi-view images featuring people, our approach combines data-driven scene reconstruction with the traditional *Structure-from-Motion (SfM)* framework to enhance the accuracy of scene and camera reconstruction while simultaneously estimating human meshes. The reconstruction process is initialized using robust foundational models for scene reconstruction [53] and human reconstruction [16] and further refined through joint optimization. This optimization incorporates a global alignment loss on scene pointmaps and bundle adjustment based on 2D human keypoint predictions [59], significantly enhancing the accuracy of the three components of world reconstruction—humans, scenes, and cameras. Our overall pipeline is depicted in Figure 2.

Unlike existing approaches to multi-view scene reconstruction [41, 42, 53, 60] and human pose estimation [8, 23, 55], HSfM recovers the metric scale of scene point clouds and camera poses while situating human meshes within a unified world coordinate system. The comprehensive output of HSfM facilitates the capture and evaluation of spatial relationships among individuals, ensuring consistency with the surrounding environment. Furthermore, unlike prior multi-view human pose estimation methods that depend on precise camera calibration [12, 20, 64], our approach operates with minimal constraints on the capture setup and does

not require prior knowledge of the environment.

Our approach is founded on two key insights. The first insight is that deep learning-based human mesh estimation inherently contains metric scale information, as the predictions reflect the statistical human size present in the training datasets, thereby constraining the scale of the scene. The second insight is that robust 2D human keypoint predictions and 3D human mesh estimations provide precise correspondences and reliable initial 3D structures for bundle adjustment. Note that for the purpose of this work, we assume known re-identification of people across camera views.

We evaluate our approach on two challenging benchmarks, *EgoHumans* [24] and *EgoExo4D* [17], which feature individuals participating in a variety of indoor and outdoor activities across diverse environments. We assess the accuracy of human mesh reconstruction by comparing our method to other approaches that estimate human poses in a world coordinate frame [56]. Additionally, we compare camera pose accuracy against learning-based dense scene reconstruction methods, such as *DUST3R* [53] and *MASt3R* [26]. Our approach demonstrates substantial improvements in camera pose estimation compared to existing methods while accurately positioning individuals within the scene. Specifically, it achieves approximately a 3.5-fold improvement in human metrics, reducing the human world location error from 3.51m to 1.04m on *EgoHumans*, and delivers camera metric improvements of approximately 2.5 times compared to the most relevant baseline [55]. These results underscore the effectiveness of our method, which leverages the joint reconstruction of multiple human meshes, scene point clouds, and cameras, supported by robust initialization for humans [16] and cameras [53]. We further validate our design through ablations which show the synergy between humans, scenes, and cameras. Our qualitative results highlight that the joint optimization of people (multiple humans), places (scenes), and cameras not only enhances human localization but also improves scene reconstruction and camera pose estimation.

In summary, we present *Humans and Structure from Motion (HSfM)*, which provides a comprehensive representation of the world—encompassing people, places, and cameras—marking a step forward in understanding complex real world environments. Please find more results at the project website: muelea.github.io/hsfm.

2. Related Work

Research in multi-person mesh reconstruction and *Structure from Motion* has seen substantial progress showing remarkable domain-specific results (see Tab. 1). Building on these foundational works, our approach unifies these areas.

Structure from Motion. *Structure from Motion (SfM)* [5, 15, 19] aims to reconstruct camera poses and 3D scene geometry from a set of images by establishing

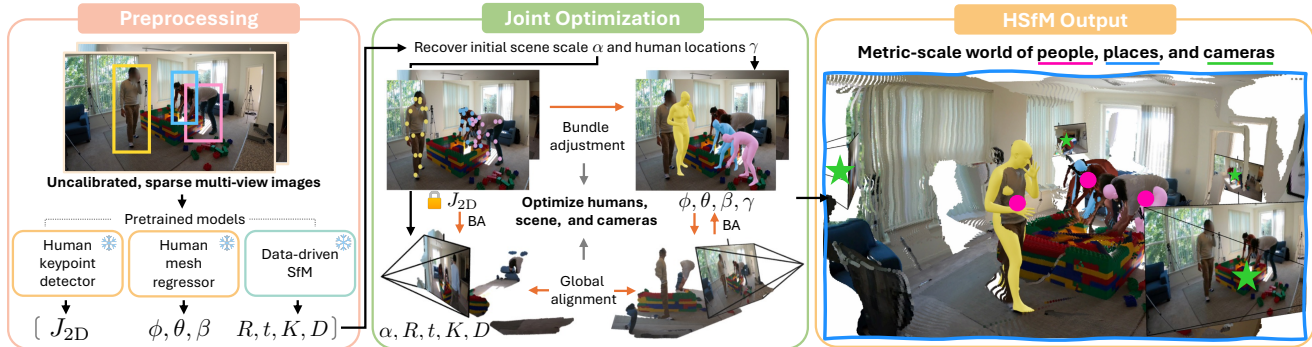


Figure 2. **Pipeline of Humans and Structure from Motion.** Our method processes synchronized images from an uncalibrated multi-view camera setup with known person correspondences across views. We utilize pretrained networks to estimate 2D human keypoints per image [59], 3D human mesh [16], scene point clouds in a *pointmap* representation, and camera intrinsic and extrinsic parameters [53]. We first initialize these estimates in a common world coordinate system by recovering the scene scale α and human locations (global translation in the world coordinate) γ , as described in Section 4.1. We then jointly optimize humans, the scene, and cameras using bundle adjustment based on 2D human keypoints, 3D human meshes, and a global alignment loss that merges per-view pointmaps into the same world space.

	Local Pose	Multi-Person	Stat. Scale	Camera	Places
HMR2 [16, 23]	✓	✗	✗	✗	✗
Multi-HMR [2]	✓	✓	✓	✗	✗
SLAHMR [61]	✓	✓	✓	✓	✗
UnCaliPose [55]	✓	✓	✓	✓	✗
DUST3R [53]	✗	✗	✗	✓	✓
MAS3R [26]	✗	✗	✓	✓	✓
HSfM	✓	✓	✓	✓	✓

Table 1. **Comparison of methods across different features.** Previous works in human pose estimation like HMR2, SLAHMR, Multi-HMR, and UnCaliPose has made great progress in reconstructing body poses in single- and multi-person setups from images. Recent methods like DUST3R and MAS3R are able to recover accurate camera poses and scene points clouds (places). This includes reconstructions with statistically correct scale (Stat. Scale) which can be obtained from human body models, *e.g.* in SLAHMR, or, as in MAS3R, from world knowledge. Our approach, HSfM, is the first method that can jointly reconstruct multiple people, scene, and cameras from sparse uncalibrated multi-view images.

pixel correspondences across views. Traditional SfM Methods [1, 9, 10], such as COLMAP [41, 42] employ keypoint detection, matching based on locally invariant descriptors [4, 30, 40], and incremental bundle adjustment to estimate camera poses and sparse 3D points. However, these traditional approaches are highly sensitive to noise at each stage of their sequential pipeline and require specific conditions for input, such as a large number of camera views with substantial overlapping image areas.

Learning-based SfM methods replace one or more components of the traditional SfM pipeline with data-driven approaches [3, 11, 28, 39, 62]. Recently, dense matching-based SfM [7, 21, 45, 50, 51, 69] has shifted from sparse keypoints to dense, data-driven approaches. DUST3R [53]

and more recent works [13, 26] exemplify this by predicting dense 3D pointmaps without requiring camera calibration. However, as these methods primarily focus on scene structure, they do not estimate human poses and face challenges in reconstructing pixels corresponding to people. In contrast, our approach robustly recovers both human poses and scene structure simultaneously.

SfM with Humans. Several recent works have leveraged humans in the scene as cues to overcome the limitations of traditional Structure from Motion (SfM) methods in challenging scenarios with minimal overlap or wide baselines. Ma et al. [32, 36] introduce the concept of Virtual Correspondences (VCs), which are pairs of pixels from different images whose camera rays intersect in 3D space, even if the points are not co-visible. Similarly, Xu et al. [58] addressed wide-baseline multi-camera calibration by employing 2D keypoint associations from people across different cameras, obtained by person re-identification methods. Xu and Kitani [56] extended this work by sequentially solving for person re-identification, camera pose estimation, and 3D human pose estimation using multi-view geometry and bundle adjustment in an optimization pipeline. While our approach aligns with this line of research, it differs by jointly optimizing people, places (scene pointmaps), and cameras.

Multi-view human reconstruction. In controlled environments with known camera parameters, multi-view reconstruction leverages geometric consistency for accurate 3D pose estimation, reducing single- and multi-person tasks to a triangulation problem [49] with a long history of research. Recent works explore setups with unknown camera poses by employing end-to-end learning methods that jointly estimate camera parameters and 3D poses [18, 63]. However, these methods are often limited to single-person scenarios [63] or do not incorporate scene context [18]. Ex-

isting multi-person methods focus on re-identification [6, 12, 22] or, for video, on re-identification and tracking [20]. In contrast to previous work, our approach does not require camera calibration. Instead, we leverage the human body structure and data-driven SfM methods to achieve accurate human pose and camera estimates.

3. Preliminaries and Notation

Setup. Our method takes as input an uncalibrated, sparse set of C images capturing people in a scene at a single moment in time. We denote each image as I^c , $c = \{1 \dots C\}$, corresponding to each camera, with resolution $H^c \times W^c$. We assume humans have been associated across views. Given this input, our method jointly reconstructs humans, scene, and cameras in a metric 3D world.

Human. For all of the following, we represent humans in the scene via a human body model, SMPL-X [35]. SMPL-X is a differentiable function that maps pose, $\theta \in \text{SO}(3)^J$, and shape, $\beta \in \mathbb{R}^B$ to a triangulated mesh with J joints. This mesh can be placed in the world via two additional parameters, orientation, $\phi \in \text{SO}(3)$, and translation, $\gamma \in \mathbb{R}^3$. We model multiple people, *i.e.* $h \in \{1 \dots H\}$ humans. In summary, a human, h , in the world is defined via

$$H^h = \{\phi^h, \theta^h, \beta^h, \gamma^h\}. \quad (1)$$

Cameras. To project 3D points onto an image, $I \in \mathbb{R}^{H \times W \times 3}$, we use a perspective camera model with intrinsics, $K \in \mathbb{R}^{3 \times 3}$ with focal lengths (f_x, f_y) and principal point $(W/2, H/2)$, and extrinsics with rotation, $R \in \text{SO}(3)$, and translation, $t \in \mathbb{R}^3$. Existing methods produce camera estimates that are not necessarily scaled to real-world size. To address this, we introduce a scaling parameter, α , which adjusts the distance between cameras while preserving their relative directions. With these parameters a 3D point, x^{3D} can be projected to 2D via

$$x_{2D} = K(Rx_{3D} + \alpha t). \quad (2)$$

The pixel coordinates, $(u', v') = (\frac{u}{w}, \frac{v}{w})$ are obtained from $x_{2D} = [u, v, w]^T$. K^c and R^c/t^c denote the in- and extrinsics of camera $c \in \{1, \dots, C\}$.

Scene. We represent the scene via per-view pointmaps [53], $S \in \mathbb{R}^{W \times H \times 3}$, a dense pixel-aligned 3D location for its corresponding image I in the world coordinate frame. S^c denotes the pointmap of an image c . A nice property of pointmap formulations is that we can express them through camera estimates and depth maps. For an image pixel (i, j) , its corresponding pointmap’s world coordinate can be written as

$$S_{i,j} = \alpha(R^T[K^{-1}D_{i,j}[i, j, 1]^T] - R^T t). \quad (3)$$

This formulation unprojects a pixel (i, j) using its depth value $D_{i,j}$ and K , and maps it to the world coordinate system through $R^T, -R^T t$, *i.e.* the *camera-to-world* transformation defined by R and t , and scaling.

4. Humans and Structure from Motion

Our method takes as input an uncalibrated, sparse set of images capturing people in a scene at a single moment in time. Given this input, our goal is to jointly estimate each person’s human parameters, the scene, and the camera parameters. Our key insight is that jointly reasoning about people, scene structure, and cameras improves all three aspects of reconstruction. To achieve this, we integrate the global scene optimization approach from recent scene reconstruction methods with the traditional Structure-from-Motion (SfM) formulation. This integration leverages 2D human keypoints as reliable correspondences and 3D human meshes as robust 3D structures for bundle adjustment. Please also refer to Figure 2.

Our joint optimization approach offers several key advantages. By incorporating human mesh predictions, the method introduces metric scale into the reconstruction process, leveraging statistical information about human body dimensions. The cameras and 2D human keypoints enable precise positioning of individuals within the world coordinate system, allowing for the recovery of their heights and relative distances. Additionally, correspondences of 2D human keypoints enhance camera calibration, which in turn improves scene reconstruction. The scene structure further stabilizes the camera pose registration, creating a feedback loop that refines the overall system. The result is a globally consistent reconstruction of humans, scenes, and cameras, providing a comprehensive understanding of the environment.

Since this is an under-determined problem, we take advantage of data-driven 3D human and scene reconstruction methods [16, 53] to provide initializations. In the following sections, we describe how we align these independent entities into a common world coordinate frame, followed by the joint optimization of the people, scene, and camera.

4.1. Initialization of World

The initial estimates of humans, scene structure, and cameras are derived from different networks and therefore exist in separate coordinate systems. Our objective is to align these components within a unified world coordinate system, a process we refer to as the initialization of the world. To achieve this, we estimate the metric scale that aligns the scene pointmaps and cameras with the humans.

One may simply start the optimization by setting the scale $\alpha = 1$. However, since SfM reconstructions are up-to-scale, the magnitude of t may vary significantly in every reconstruction. If the SfM scene is too small relative to peo-

ple, cameras may be in front of the humans, *e.g.* when the scene is placed inside the human mesh, leading to degenerate solutions. Setting alpha to an arbitrarily big value such as $\alpha = 100$ can prevent these issues, but makes the problem prone to local minima.

We propose an analytical method to approximate a consistent reconstruction using data-driven outputs of 2D/3D human keypoints and camera parameters. Initially, we roughly position individuals within the scene by estimating γ , based on the predicted 2D/3D human keypoints and the focal length from \tilde{K} , following a similar approach to Ye et al. [61]. Next, we calculate the initial scale α of the data-driven SfM-predicted world by aligning the data-driven camera positions with human-centric camera positions.

Specifically, we first obtain each camera’s rotation, \hat{R}^c , using the estimated 3D human body orientation, $\tilde{\phi}$. This leverages the fact that the human’s orientation should remain consistent in the world coordinate frame across different views. Assuming a reference camera, c_1 , and an anchor person, $\tilde{\phi}^h$, we recover each camera’s rotation by solving

$$(\hat{R}^c)^\top = (R^{c_1})^\top \tilde{\phi}^{hc_1} (\tilde{\phi}^{hc})^\top. \quad (4)$$

We pick the anchor person h based on the best view coverage w.r.t. to the 2D joint confidence scores.

We estimate the camera translation by first estimating the location of the person γ in the world using the data-driven focal length prediction from \tilde{K} and the size of the predicted human following the similar triangle ratio using the average 2D and 3D bone lengths as done in Ye *et al.* [61]. Because the human position in the world coordinate frame should remain consistent when viewed from any camera, we recover camera position T^c in the world coordinate frame via

$$\hat{T}^c = \tilde{\gamma}^{c_1} - (\hat{R}^c)^\top \tilde{\gamma}^c. \quad (5)$$

Finally, given the camera positions \hat{T} derived from the humans and the data-driven camera position predictions \tilde{T} , we solve a least-squares problem to compute $\hat{\alpha}$, which aligns the scene pointmap \mathcal{S} and the camera translation t with the metric-scale world defined by the humans \tilde{H} . The scaling factor $\hat{\alpha}$ provides a reasonable approximation of the metric scale. For the initial estimates of \tilde{H} , we rely on an estimate from a reference camera in practice. Please refer to the supplementary video on our project page for an animated illustration of this approach.

4.2. Reconstructing People, Places, and Cameras

After initializing the world, we jointly optimize the humans, depth maps, and cameras using a global scene optimization loss and bundle adjustment guided by 2D human keypoint

predictions. The objective function is defined as follows:

$$\min_{\{\alpha, \gamma, \beta, \phi, \theta, R, t, K, D\}} L_{\text{Humans}} + \lambda L_{\text{Places}}. \quad (6)$$

To gradually guide the optimization towards the global minimum, we first optimize $\{\alpha, \gamma, \beta\}$ with $\lambda = 0$. Then, we set λ and optimize $\{\gamma, \beta, \phi, \theta, R, t, K, D\}$. The result of this optimization is a metric-scale world with consistent humans, scene, and cameras.

Bundle adjustment based on human keypoints: We define the bundle adjustment objective as follows:

$$L_{\text{Humans}} = \frac{1}{HC} \sum_{c=1}^C \sum_{h=1}^H L_J^{ch} + \frac{1}{H} \sum_{h=1}^H L_\beta^h. \quad (7)$$

The term L_J denotes the re-projection error between the 3D joints of the current estimate with the estimated camera and detected 2D keypoints by ViTPose [59]:

$$L_J^{ch} = \frac{1}{b_{2D}^{ch}} \|c_{2D}^{ch}(J_{2D}^{ch} - K^c(R^c J_{3D}^h + \alpha t^c))\|_2 \quad (8)$$

The keypoint loss for each person, h , and camera, c , is normalized by the bounding box height b_{2D}^{ch} of the 2D human detection and detected keypoints weighted by their estimated confidence scores c_{2D}^{ch} . We further regularize human body shape, β , to stay close to the average shape of the human body model:

$$L_\beta^h = \|\beta^h\|_2. \quad (9)$$

The output of this optimization is people in plausible size and locations in the world coordinate frame. Please refer to the supplementary material for implementation details.

Global scene optimization: We adapt the global alignment loss from DUST3R [53], which originally optimizes camera and world pointmaps.

Intuitively, this loss takes pairs of cameras, say Alice and Bob (c_i and c_j), with the predicted content of Alice in Bob’s view. The alignment loss transforms this “Alice’-content-in-Bob’s-view” to the world coordinate frame where it’s compared against the optimized global scene pointmap, which is Alice’s content in the world.

More formally, the global alignment loss aligns per-view pointmaps into a joint world space, *i.e.* $\{\mathcal{S}^c \in \mathbf{R}^{H \times W \times 3}\}$ for $c = 1 \dots C$. To achieve this, the alignment loss takes cross-view pointmaps X^{c_i, c_j} for two cameras $(c_i, c_j) \in \mathcal{E}$, with $i, j = 1 \dots C$ and \mathcal{E} being the set of all pairs of cameras with $i \neq j$. The notation, X^{c_i, c_j} , describes cross-view pointmaps, meaning that the pointmap X^{c_i} of camera c_i is expressed in the coordinate frame of camera c_j . Pairwise transformation matrices $P^{c_i, c_j \rightarrow w} \in \mathbb{R}^{3 \times 4}$, *i.e.* the transformation matrix for camera pair c_i, c_j that brings c_j ’s content to the world coordinate frame. The global alignment loss term is defined as

$$L_{\text{Places}} = \sum_{(c_i, c_j) \in \mathcal{E}} \sum_{i=1}^{HW} Q_i^{c_i, c_j} \|\mathcal{S}_i^{c_i} - \sigma^{c_i, c_j \rightarrow w} P^{c_i, c_j \rightarrow w} X_i^{c_i, c_j}\|, \quad (10)$$

where $Q_i^{c_i, c_j}$ are predicted per-pixel confidence maps. $\sigma^{c_i, c_j \rightarrow w}$ is a scaling factor associated to the pair (c_i, c_j) . Note that different from DUST3R [53], we don’t regularize it to avoid a trivial optimum, since the scale is constrained by humans. We omit σ and P in Eq. 6 for clarity, but they are still optimized together following DUST3R.

5. Experiments

We evaluate the effectiveness of our approach in terms of human pose estimation within the world coordinate system and camera accuracy. Additionally, we present qualitative results showcasing the effects of our joint optimization on humans, scene pointmaps, and cameras.

5.1. Evaluation

Evaluation Datasets: We evaluate on the EgoHumans [24] and EgoExo4D [17] datasets. EgoHumans is a new multi-view, multi-human video benchmark designed for egocentric 3D human pose estimation and tracking. It captures over 125,000 images of two to four people interacting in dynamic, real-world activities. EgoExo4D is a large-scale, multi-view video dataset comprising simultaneously captured egocentric and exocentric videos of skilled human activities such as sports, music, dance, and bike repair for a single person. Please refer to the supplementary material for more details.

Evaluation Metrics: We report metrics for humans and cameras. For people, we use the Mean Per-Joint Position Error (MPJPE). We report **W-MPJPE**, the metric measured in the world coordinate system, and **PA-MPJPE**, its Procrustes-Aligned version, measuring the local pose accuracy. We introduce Group-Aligned MPJPE, (**GA-MPJPE**), which evaluates the relative distance after Sim(3) alignment between people. All metrics are reported in meters.

For cameras, we report average camera translation error **TE**, *i.e.* the mean Euclidean distance in meters between predicted and ground truth camera translations after SE(3) alignment. TE evaluates accuracy in the metric prediction. We also report the Sim(3) aligned version, **s-TE**. **AE** measures the camera Angle Error, *i.e.* the mean Euclidean distance between predicted and ground truth camera rotation. **RRA** [52] evaluates the Relative Rotation Accuracy by comparing the relative rotation between two predicted cameras with the corresponding ground truth. **CCA** [27] assesses the Camera Center Accuracy by directly comparing the predicted and ground truth camera poses. While Lin et al. [27] reported CCA only after optimal Sim(3) alignment, we provide results for two variants: the default

metric computed after SE(3) alignment, and **s-CCA**, computed after Sim(3) alignment. RRA, CCA, and s-CCA are reported for a threshold τ following the previous literature [13, 27, 52, 53]. Note that W-MPJPE, TE, and CCA evaluate absolute Euclidean error, while GA-MPJPE, PA-MPJPE, s-TE, and s-CCA evaluate errors up to scale. For further details, please refer to the supplementary material.

5.2. Results

We report the results in Tab. 2, comparing various human and camera estimation baselines on EgoHumans and EgoExo4D. We evaluate human and camera estimates against UnCaliPose [55], and camera estimates against DUST3R [53] and MAST3R [26]. UnCaliPose is the closest baseline, as it uses humans for Structure-from-Motion (SfM) and jointly reconstructs both humans and cameras. However, it does not reconstruct the scene, and the scale is recovered using ground truth bone lengths during testing. For a fair comparison, we assume known re-identification across views and use ViTPose [59] for both UnCaliPose and HSfM. Additionally, we use the predicted focal length from DUST3R [53] for UnCaliPose. Since no method exists that jointly estimates people, places, and cameras at metric scale from sparse multi-view images, we further report results on HSfM (init.), *i.e.* the world state after the initialization procedure described in Sec. 4.1.

As shown in the EgoHumans table, HSfM (init.) outperforms UnCaliPose in scale-normalized human metrics, reducing GA-MPJPE by approximately 24% and PA-MPJPE by over 50%. Additionally, HSfM (init.) achieves a relative rotation accuracy that is nearly double, with RRA@10 improving by 86% and RRA@15 by over 100% compared to UnCaliPose. This demonstrates the effectiveness of our strong initialization, which leverages foundational models—HMR2 for humans and DUST3R for cameras.

Our optimization yields substantial improvements. For instance, W-MPJPE is reduced from 4.28m in HSfM (init.) to 1.04m in HSfM, demonstrating the effectiveness of our approach in resolving scale ambiguity and accurately positioning humans within the world. Additionally, the camera metrics show significant enhancements. Our method surpasses the initial outputs of DUST3R and outperforms MAST3R in metric-scale camera metrics with large margins, reducing TE from 4.97m to 2.09m and achieving approximately seven times better CCA@15. These results highlight the advantages of incorporating humans into the reconstruction process to achieve a consistent metric-scale world, consistent with the findings of Zhao et al. [67].

Similar trends are observed in the EgoExo4D results, further validating the effectiveness of our method in reconstructing the world. HSfM achieves substantially better human metrics compared to UnCaliPose, reducing W-MPJPE from 2.90m to 0.56m and PA-MPJPE from 0.13m to 0.06m.

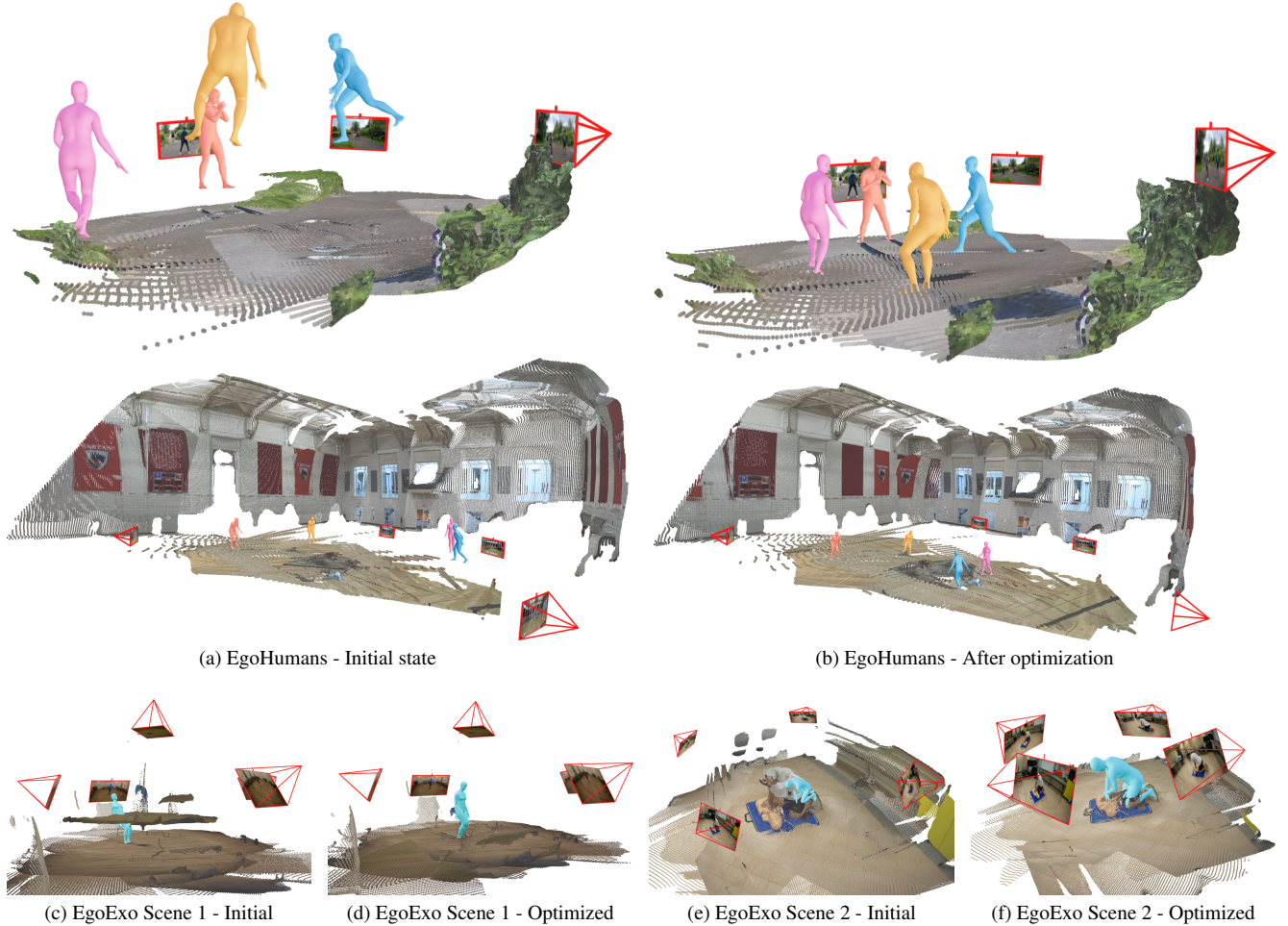


Figure 3. **Qualitative results from HSfM.** We show our optimized result on sequences from EgoHumans (top) and EgoExo4D (bottom). Note how in the Initial state (left) people are floating in the air (a), how the scene and human scale is not aligned (e), and how noisy the scene appears (c). Our method resolves these problems by grounding people in the scene (b), recovering plausible metric scale (f), and better camera estimates (d). We achieve this with minimal assumptions and without scene contact constraints.

Method	Human Metrics							Camera Metrics					
	W-MPJPE↓	GA-MPJPE↓	PA-MPJPE↓	TE↓	s-TE↓	AE↓	RRA@10↑	RRA@15↑	CCA@10↑	CCA@15↑	s-CCA@10↑	s-CCA@15↑	
EgoHumans													
UnCaliPose* [55]	3.51	0.67	0.13	2.63	2.63	60.90	0.28	0.39	-	-	0.33	0.44	
DUST3R [53]	-	-	-	-	1.15	11.00	0.61	0.74	-	-	0.49	0.74	
MASt3R [26]	-	-	-	4.97	0.92	10.42	0.61	0.74	0.06	0.07	0.65	0.86	
HSfM (init.)	4.28	0.51	0.06	2.37	1.15	11.00	0.52	0.79	0.26	0.38	0.49	0.74	
HSfM (Ours)	1.04	0.21	0.05	2.09	0.75	9.35	0.72	0.89	0.32	0.46	0.75	0.91	
EgoExo4D													
UnCaliPose* [55]	2.90	-	0.14	2.43	1.16	65.61	0.19	0.29	-	-	0.24	0.34	
DUST3R [53]	-	-	-	-	0.33	9.92	0.81	0.88	-	-	0.64	0.85	
MASt3R [26]	-	-	-	0.96	0.35	11.70	0.79	0.87	0.06	0.14	0.68	0.81	
HSfM (init.)	5.29	-	0.07	1.27	0.33	9.92	0.81	0.88	0.05	0.09	0.64	0.85	
HSfM (Ours)	0.56	-	0.06	0.95	0.36	11.57	0.78	0.87	0.07	0.16	0.67	0.82	

Table 2. **Evaluation on EgoHumans and EgoExo4D.** HSfM outperforms existing human and scene reconstruction methods, delivering metric-scale reconstructions for humans, the scene, and cameras within the same world coordinate system. Our approach shows major improvement over the initial estimates HSfM (init.), obtained from DUST3R [53] and HMR2 [16] (Section 4.1), particularly when multiple humans are present in the scene, as seen in EgoHumans, compared to a single individual in EgoExo4D. Additionally, HSfM surpasses MASt3R in metric-scale camera metrics, demonstrating the benefit of incorporating humans into the Structure-from-Motion (SfM) pipeline for scale recovery. All baselines and our method use four cameras as input on EgoHumans and up to six cameras on EgoExo4D. Human metrics and camera translation metrics are reported in meters.

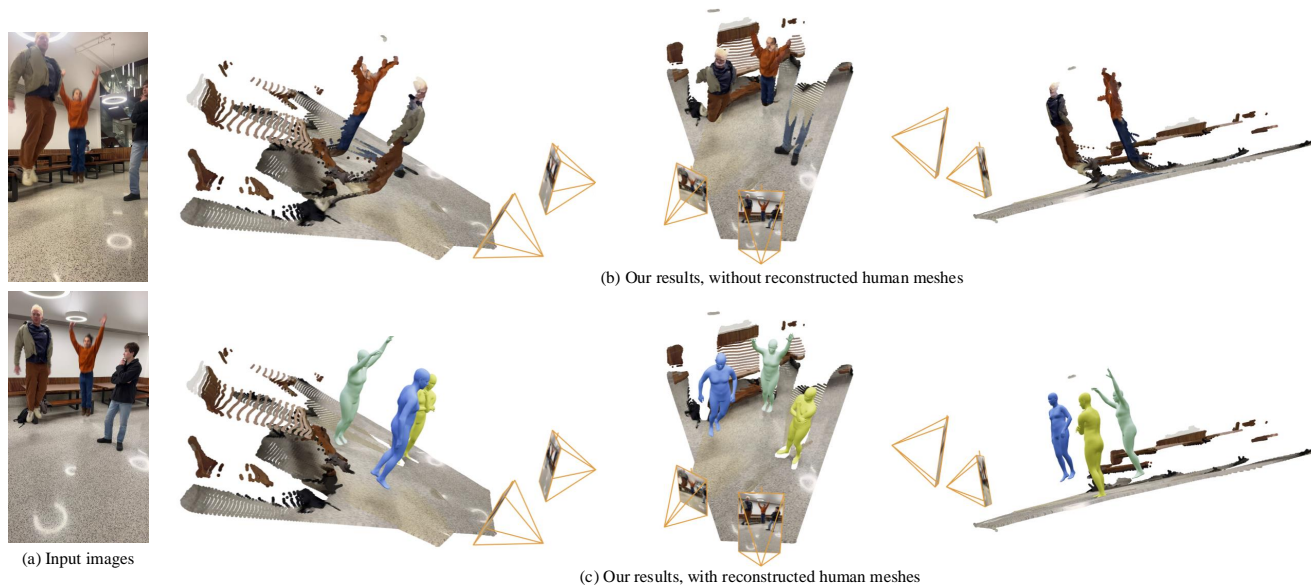


Figure 4. **Qualitative results in the wild.** We show reconstructions on *in-the-wild* images taken with two smartphones (a), demonstrating the reconstruction of humans and scenes. Unlike previous works [61, 70], which adopt human-scene contact priors that hinder generalization to scenarios without ground foot contact, HSfM recovers accurate world locations of the human meshes that are coherent with the static scene structure. The use of humans in our framework (c) not only serves as a reliable initialization for 3D structure in the SfM formulation but also provides more faithful and complete information about people in the world, which a noisy human point cloud (b) cannot offer. For visualization purposes, the human point cloud is removed using SAM2 [38].

Method	Human Metrics						Camera Metrics					
	W-MPJPE↓	GA-MPJPE↓	PA-MPJPE↓	TE↓	s-TE↓	AE↓	RRA@10↑	RRA@15↑	CCA@10↑	CCA@15↑	s-CCA@10↑	s-CCA@15↑
M0: HSfM (init.)	4.28	0.51	0.06	2.37	1.15	11.00	0.52	0.79	0.26	0.38	0.49	0.74
M1: S & C w/o L_{Humans}	3.94	0.57	0.10	2.13	1.1	10.93	0.52	0.79	0.27	0.40	0.48	0.77
M2: w/o L_{Places}	1.29	0.24	0.05	2.82	0.87	13.02	0.50	0.73	0.16	0.24	0.72	0.88
M3: HSfM (Ours)	1.04	0.21	0.05	2.09	0.75	9.35	0.72	0.89	0.32	0.46	0.75	0.91
HSfM (init.)	3.87	0.70	0.06	1.88	1.15	11.34	0.47	0.77	0.23	0.37	0.38	0.69
1 Human	1.69	0.58	0.06	1.91	1.21	10.31	0.52	0.82	0.27	0.44	0.44	0.68
2 Humans	1.66	0.49	0.06	1.84	1.10	9.41	0.62	0.87	0.33	0.45	0.53	0.75
3 Humans	1.41	0.38	0.06	1.69	0.93	8.21	0.74	0.92	0.32	0.46	0.58	0.78
4 Humans	1.28	0.39	0.06	1.52	0.77	8.11	0.74	0.90	0.34	0.53	0.73	0.90

Table 3. **Ablation study.** We demonstrate the advantages of our joint optimization by removing each terms on the EgoHumans dataset. The results indicate that joint optimization is crucial for achieving a coherent reconstruction of cameras and humans. We also perform an ablation study to investigate how the number of humans included affects both camera and human pose estimation in the world coordinates by varying the number of people to include in the optimization using a subset of EgoHumans containing scenes with four people. The results reveal that the effect scales with the number of humans, highlighting the importance of leveraging multiple individuals.

For metric-scale camera metrics, HSfM outperforms both MAST3R and HSfM (init.), improving CCA@15 by 14% and 78%, respectively.

However, the improvements, especially in scale-invariant camera metrics (e.g., RRA@10/15) are less compared to those observed in EgoHumans. This reduced performance is likely due to two factors: significant occlusions in indoor images, which affect 2D human keypoint predictions, and the fact that only a single person is used for optimization in EgoExo4D. In contrast, EgoHumans utilizes

multiple individuals, providing a greater number of 2D human keypoint correspondences, which strengthens the optimization process. Our ablation study confirms this trend.

Ablations: We first validate the importance of our joint optimization of humans, scenes, and cameras in Table 3. The first variant, M1, detaches the gradients from the human loss to the scene and camera parameters while still optimizing all parameters. Essentially, the cameras and scene do not adjust to minimize the human losses. This leads to W-MPJPE improving only marginally from the initializa-

tion (4.28m to 3.94m) and GA-MPJPE slightly increasing to 0.57m from 0.51m. Since human losses do not influence the optimization of the camera and scene, the camera metrics also stagnate, with RRA@15 showing no improvement, and CCA@15 increasing only marginally by 5.3%. The second variant, M2, optimizes cameras and humans solely based on the human loss, excluding the scene loss. Interestingly, this significantly improves W-MPJPE from 4.28m to 1.29m and GA-MPJPE from 0.57m to 0.24m, indicating accurate recovery of human world locations and relative distances. However, the camera metrics degrade considerably: CCA@15 decreases by 36.8%, and RRA@15 declines by 7.6%. This highlights that without incorporating scene losses, the structure fails to anchor the cameras, leading to overfitting to human keypoints. This behavior is similar to the limitations observed in UnCaliPose, which relies solely on human keypoints for Structure-from-Motion (SfM). In contrast, our full method (M3: HSfM (Ours)) achieves the best performance across all metrics, reducing W-MPJPE to 1.04m, GA-MPJPE to 0.21m, and improving camera metrics, with RRA@15 increasing by 22% and CCA@15 by 21%. These results underscore the critical importance of jointly optimizing humans, scenes, and cameras to achieve a coherent and accurate metric-scale reconstruction.

We conduct an ablation study to investigate the impact of the number of humans on camera estimation and its subsequent effect on human metrics in the world coordinate system. As shown in the table, adding more humans consistently improves camera pose estimation, particularly by reducing camera translation error. This improvement directly contributes to achieving the lowest W-MPJPE, accurately reconstructing human locations in the world.

The results highlight that increasing the number of humans introduces more correspondences for Structure-from-Motion (SfM), thereby strengthening the bundle adjustment process. This validates our strategy of integrating global scene optimization techniques from recent scene reconstruction methods with the traditional SfM formulation. Our approach effectively leverages 2D human keypoints as reliable correspondences and 3D human meshes as robust structures to enhance bundle adjustment and produce coherent, metric-scale reconstructions. Please refer to the supplementary material for the ablation study on camera/scene scale initialization and the impact of the number of cameras.

Qualitative Results: See Figure 1 and Figure 3 for qualitative results on EgoHumans and EgoExo4D, and Figure 4 for reconstructions on images taken in the wild.

Figure 3 shows the intermediate steps of the optimization, where in the beginning, people are floating around in mid air. After the optimization, their feet are consistent with the environment, without any explicit contact constraints. We see that the structure also improves — the pointmaps

are more coherent around the ground.

Lastly, in Figure 4, we present visualizations of HSfM’s outputs on in-the-wild images. The data was captured using a minimal setup consisting of two cell phones, two tripods, and the Riverside app¹ for straightforward time synchronization. Despite this simple setup, our multi-view optimization algorithm successfully handles challenging scenes, such as individuals jumping, without relying on any heuristic contact priors and small data-driven motion priors that previous works [44, 61, 68] use. Please refer to the supplementary material for more qualitative results.

6. Conclusion

In this work, we propose Humans and Structure from Motion, HSfM, which optimizes humans, scene, and cameras in a joint framework. We build on the success of data-driven learning in two parallel domains – 2D/3D human reconstruction [16, 59] and scene reconstruction [53]. However, neither of these approaches is able to reconstruct humans, scenes, and cameras coherently. Our experiments verify the synergy between these three elements — integrating human reconstruction into the classic Structure from Motion task not only properly places people in the world, but also significantly improves camera pose accuracy. While our approach gives promising results, it is an optimization-based framework and can be sensitive to hyper-parameters. In future work, it would be interesting to explore this synergy in a feed-forward framework. It will also be exciting to extend this insight into videos.

7. Acknowledgements:

This project is supported in part by DARPA No. HR001123C0021, IARPA DOI/IBC No. 140D0423C0035, NSF:CNS-2235013, ONR MURI N00014-21-1-2801, Bakar Fellows, and Bair Sponsors. The views and conclusions contained herein are those of the authors and do not represent the official policies or endorsements of these institutions. We also thank Chung Min Kim for her critical reviews of this paper and Junyi Zhang for his valuable insights on the method.

References

- [1] Sameer Agarwal, Yasutaka Furukawa, Noah Snavely, Ian Simon, Brian Curless, Steven M Seitz, and Richard Szeliski. Building rome in a day. *ACM Communications*, 2011. 3
- [2] Fabien Baradel, Matthieu Armando, Salma Galaoui, Romain Brégier, Philippe Weinzaepfel, Grégory Rogez, and Thomas Lucas. Multi-hmr: Multi-person whole-body human mesh recovery in a single shot. *arXiv preprint arXiv:2402.14654*, 2024. 3, 4

¹<https://riverside.fm/>

- [3] Axel Barroso-Laguna, Edgar Riba, Daniel Ponsa, and Krystian Mikolajczyk. Key.net: Keypoint detection by hand-crafted and learned cnn filters. In *International Conference on Computer Vision (ICCV)*, 2019. 3
- [4] Herbert Bay, Tinne Tuytelaars, and Luc Van Gool. Surf: Speeded up robust features. In *European Conference on Computer Vision (ECCV)*, 2006. 3
- [5] Paul Beardsley, Phil Torr, and Andrew Zisserman. 3d model acquisition from extended image sequences. In *European Conference on Computer Vision (ECCV)*, 1996. 2
- [6] Chao Chen, Georgios Pavlakos, Shihao Zou, Tony Tung, and Katerina Fragkiadaki. Multi-person 3d pose estimation in crowded scenes based on multi-view geometry. *arXiv preprint arXiv:2007.10986*, 2020. 4
- [7] Hongkai Chen, Zixin Luo, Lei Zhou, Yurun Tian, Mingmin Zhen, Tian Fang, David McKinnon, Yanghai Tsin, and Long Quan. Aspanformer: Detector-free image matching with adaptive span transformer. In *European Conference on Computer Vision (ECCV)*, 2022. 3
- [8] Hongsuk Choi, Gyeongsik Moon, and Kyoung Mu Lee. Pose2mesh: Graph convolutional network for 3d human pose and mesh recovery from a 2d human pose. In *European Conference on Computer Vision (ECCV)*, 2020. 2
- [9] David Crandall, Andrew Owens, Noah Snavely, and Daniel Huttenlocher. Sfm with mrfs: Discrete-continuous optimization for large-scale structure from motion. *IEEE Transactions on Pattern Analysis and Machine Intelligence (PAMI)*, 2013. 3
- [10] Hainan Cui, Xiang Gao, Shuhan Shen, and Zhanyi Hu. Hsfm: Hybrid structure-from-motion. In *Proceedings of the IEEE Conference on Computer Vision and Pattern Recognition (CVPR)*, 2017. 3
- [11] Daniel DeTone, Tomasz Malisiewicz, and Andrew Rabynovich. Superpoint: Self-supervised interest point detection and description. In *CVPR Workshops*, 2018. 3
- [12] Junting Dong, Hujun Bao, and Xiaowei Zhou. Fast and robust multi-person 3d pose estimation from multiple views. In *Proceedings of the IEEE/CVF Conference on Computer Vision and Pattern Recognition (CVPR)*, pages 7792–7801, 2019. 2, 4
- [13] Bardienu Duisterhof, Lojze Zust, Philippe Weinzaepfel, Vincent Leroy, Yohann Cabon, and Jerome Revaud. Mast3r-sfm: A fully-integrated solution for unconstrained structure-from-motion. *arXiv preprint arXiv*, 2024. 3, 6
- [14] Sai Kumar Dwivedi, Yu Sun, Priyanka Patel, Yao Feng, and Michael J. Black. TokenHMR: Advancing human mesh recovery with a tokenized pose representation. In *IEEE/CVF Conference on Computer Vision and Pattern Recognition (CVPR)*, 2024. 4
- [15] Andrew W Fitzgibbon and Andrew Zisserman. Automatic camera recovery for closed or open image sequences. In *European Conference on Computer Vision (ECCV)*, 1998. 2
- [16] Shubham Goel, Georgios Pavlakos, Jathushan Rajasegaran, Angjoo Kanazawa*, and Jitendra Malik*. Humans in 4D: Reconstructing and tracking humans with transformers. In *International Conference on Computer Vision (ICCV)*, 2023. 2, 3, 4, 7, 9, 1
- [17] Kristen Grauman, Andrew Westbury, Lorenzo Torresani, Kris Kitani, Jitendra Malik, Triantafyllos Afouras, Kumar Ashutosh, Vijay Baiyya, Siddhant Bansal, Bikram Boote, et al. Ego-exo4d: Understanding skilled human activity from first-and third-person perspectives. In *Proceedings of the IEEE/CVF Conference on Computer Vision and Pattern Recognition*, 2024. 2, 6, 1
- [18] Peter Hardy and Hansung Kim. Unsupervised multi-person 3d human pose estimation from 2d poses alone. *arXiv preprint arXiv:2309.14865*, 2023. 3
- [19] Richard Hartley and Andrew Zisserman. *Multiple View Geometry in Computer Vision*. 2004. 2
- [20] Chun-Hao P. Huang, Hongwei Yi, Markus Höschle, Matvey Safroshkin, Tsvetelina Alexifadis, Senya Polikovsky, Daniel Scharstein, and Michael J. Black. Capturing and inferring dense full-body human-scene contact. In *2022 IEEE/CVF Conference on Computer Vision and Pattern Recognition (CVPR 2022)*, pages 13264–13275, 2022. 2, 4
- [21] Wei Jiang, Eduard Trulls, Jan Hosang, Andrea Tagliasacchi, and Kwang Moo Yi. Cotr: Correspondence transformer for matching across images. In *International Conference on Computer Vision (ICCV)*, 2021. 3
- [22] Amir Kadkhodamohammadi and Nicolas Padoy. A generalizable approach for multi-view 3d human pose regression. *arXiv preprint arXiv:1804.10462*, 2018. 4
- [23] Angjoo Kanazawa, Michael J. Black, David W. Jacobs, and Jitendra Malik. End-to-end recovery of human shape and pose. In *Computer Vision and Pattern Recognition (CVPR)*, pages 7122–7131, 2018. 2, 3, 4
- [24] Rawal Khirodkar, Aayush Bansal, Lingni Ma, Richard Newcombe, Minh Vo, and Kris Kitani. Egohumans: An egocentric 3d multi-human benchmark. *arXiv preprint arXiv:2305.16487*, 2023. 2, 6, 1
- [25] Diederik P. Kingma and Jimmy Ba. Adam: A method for stochastic optimization. In *International Conference on Learning Representations (ICLR)*, 2015. 4
- [26] Vincent Leroy, Yohann Cabon, and Jerome Revaud. Grounding image matching in 3d with mast3r. In *European Conference on Computer Vision (ECCV)*, 2024. 2, 3, 6, 7
- [27] Amy Lin, Jason Y Zhang, Deva Ramanan, and Shubham Tulsiani. Relpose++: Recovering 6d poses from sparse-view observations. *arXiv preprint arXiv:2305.04926*, 2023. 6, 3
- [28] Philipp Lindenberger, Paul-Edouard Sarlin, and Marc Pollefeys. Lightglue: Local feature matching at light speed. In *International Conference on Computer Vision (ICCV)*, 2023. 3
- [29] Miao Liu, Dexin Yang, Yan Zhang, Zhaopeng Cui, James M Rehg, and Siyu Tang. 4d human body capture from egocentric video via 3d scene grounding. In *3DV*, 2021. 4
- [30] David G. Lowe. Distinctive image features from scale-invariant keypoints. *International Journal of Computer Vision (IJCV)*, 2004. 3
- [31] Hao Luo, Youzhi Gu, Xingyu Liao, Shenqi Lai, and Wei Jiang. Bag of tricks and a strong baseline for deep person re-identification. In *Proceedings of the IEEE/CVF Conference on Computer Vision and Pattern Recognition Workshops*, 2019. 1

- [32] Wei-Chiu Ma, Alexander J. Yang, Shenlong Wang, Raquel Urtasun, and Antonio Torralba. Virtual correspondence: Humans as a cue for extreme-view geometry. In *Proceedings of the IEEE/CVF Conference on Computer Vision and Pattern Recognition (CVPR)*, 2022. 3
- [33] Lea Müller, Vickie Ye, Georgios Pavlakos, Michael J. Black, and Angjoo Kanazawa. Generative proxemics: A prior for 3D social interaction from images. 2024. 4
- [34] Maxime Oquab, Timothée Darcet, Théo Moutakanni, Huy Vo, Marc Szafraniec, Vasil Khalidov, Pierre Fernandez, Daniel Haziza, Francisco Massa, Alaaeldin El-Nouby, et al. Dinov2: Learning robust visual features without supervision. *arXiv preprint arXiv:2304.07193*, 2023. 1
- [35] Georgios Pavlakos, Vasileios Choutas, Nima Ghorbani, Timo Bolkart, Ahmed A. A. Osman, Dimitrios Tzionas, and Michael J. Black. Expressive body capture: 3D hands, face, and body from a single image. In *Computer Vision and Pattern Recognition (CVPR)*, pages 10975–10985, 2019. 4
- [36] Georgios Pavlakos, Jitendra Malik, and Angjoo Kanazawa. Human mesh recovery from multiple shots. In *Proceedings of the IEEE/CVF Conference on Computer Vision and Pattern Recognition*, pages 1485–1495, 2022. 3
- [37] Jathushan Rajasegaran, Georgios Pavlakos, Angjoo Kanazawa, and Jitendra Malik. Tracking people by predicting 3d appearance, location and pose. In *Proceedings of the IEEE/CVF Conference on Computer Vision and Pattern Recognition*, 2022. 1
- [38] Nikhila Ravi, Valentin Gabeur, Yuan-Ting Hu, Ronghang Hu, Chaitanya Ryali, Tengyu Ma, Haitham Khedr, Roman Rädle, Chloe Rolland, Laura Gustafson, Eric Mintun, Junting Pan, Kalyan Vasudev Alwala, Nicolas Carion, Chao-Yuan Wu, Ross Girshick, Piotr Dollár, and Christoph Feichtenhofer. Sam 2: Segment anything in images and videos. *arXiv preprint arXiv:2408.00714*, 2024. 8
- [39] Jérôme Revaud, César Roberto de Souza, Martin Humenberger, and Philippe Weinzaepfel. R2d2: Reliable and repeatable detector and descriptor. In *Advances in Neural Information Processing Systems (NeurIPS)*, 2019. 3
- [40] Ethan Rublee, Vincent Rabaud, Kurt Konolige, and Gary R. Bradski. Orb: An efficient alternative to sift or surf. In *International Conference on Computer Vision (ICCV)*, 2011. 3
- [41] Johannes Lutz Schönberger and Jan-Michael Frahm. Structure-from-motion revisited. In *Conference on Computer Vision and Pattern Recognition (CVPR)*, 2016. 2, 3
- [42] Johannes Lutz Schönberger, Enliang Zheng, Marc Pollefeys, and Jan-Michael Frahm. Pixelwise view selection for unstructured multi-view stereo. In *European Conference on Computer Vision (ECCV)*, 2016. 2, 3
- [43] Zehong Shen, Huaijin Pi, Yan Xia, Zhi Cen, Sida Peng, Zechen Hu, Hujun Bao, Ruizhen Hu, and Xiaowei Zhou. World-grounded human motion recovery via gravity-view coordinates. In *SIGGRAPH Asia 2024 Conference Papers*, pages 1–11, 2024. 4
- [44] Soyong Shin, Juyong Kim, Eni Halilaj, and Michael J. Black. WHAM: Reconstructing world-grounded humans with accurate 3D motion. In *IEEE/CVF Conf. on Computer Vision and Pattern Recognition (CVPR)*, 2024. 9, 4
- [45] Jiaming Sun, Zehong Shen, Yuang Wang, Hujun Bao, and Xiaowei Zhou. Loftr: Detector-free local feature matching with transformers. In *Conference on Computer Vision and Pattern Recognition (CVPR)*, 2021. 3
- [46] Yu Sun, Wu Liu, Qian Bao, Yili Fu, Tao Mei, and Michael J. Black. Putting people in their place: Monocular regression of 3d people in depth. In *Computer Vision and Pattern Recognition (CVPR)*, pages 13243–13252, 2022. 4
- [47] Yu Sun, Qian Bao, Wu Liu, Tao Mei, and Michael J. Black. TRACE: 5D Temporal Regression of Avatars with Dynamic Cameras in 3D Environments. In *IEEE/CVF Conf. on Computer Vision and Pattern Recognition (CVPR)*, 2023. 4
- [48] Carlo Tomasi and Takeo Kanade. Shape and motion from image streams under orthography: a factorization method. *International journal of computer vision*, 9:137–154, 1992. 2
- [49] Bill Triggs, Paul F. McLauchlan, Richard I. Hartley, and Andrew W. Fitzgibbon. Bundle adjustment—a modern synthesis. In *Vision Algorithms: Theory and Practice*, pages 298–372. Springer, Berlin, Heidelberg, 2000. 3
- [50] Prune Truong, Martin Danelljan, and Radu Timofte. Glunet: Global-local universal network for dense flow and correspondences. In *Conference on Computer Vision and Pattern Recognition (CVPR)*, 2020. 3
- [51] Prune Truong, Martin Danelljan, Luc Van Gool, and Radu Timofte. Learning accurate dense correspondences and when to trust them. In *Conference on Computer Vision and Pattern Recognition (CVPR)*, 2021. 3
- [52] Jianyuan Wang, Christian Rupprecht, and David Novotny. Posediffusion: Solving pose estimation via diffusion-aided bundle adjustment. In *International Conference on Computer Vision (ICCV)*, pages 9773–9783, 2023. 6, 3
- [53] Shuzhe Wang, Vincent Leroy, Yohann Cabon, Boris Chidlovskii, and Jerome Revaud. Dust3r: Geometric 3d vision made easy. In *Proceedings of the IEEE/CVF Conference on Computer Vision and Pattern Recognition (CVPR)*, pages 20697–20709, 2024. 2, 3, 4, 5, 6, 7, 9, 1
- [54] Yufu Wang, Ziyun Wang, Lingjie Liu, and Kostas Daniilidis. Tram: Global trajectory and motion of 3d humans from in-the-wild videos. *arXiv preprint arXiv:2403.17346*, 2024. 4
- [55] Yan Xu and Kris Kitani. Multi-view multi-person 3d pose estimation with uncalibrated camera networks. In *British Machine Vision Conference (BMVC)*, 2022. 2, 3, 6, 7
- [56] Yan Xu and Kris Kitani. Multi-view multi-person 3d pose estimation with uncalibrated camera networks. In *British Machine Vision Conference (BMVC)*, 2022. 2, 3
- [57] Yuanlu Xu, Song-Chun Zhu, and Tony Tung. DenseRaC: Joint 3D pose and shape estimation by dense render-and-compare. In *International Conference on Computer Vision (ICCV)*, 2019. 1
- [58] Yan Xu, Yu-Jhe Li, Xinshuo Weng, and Kris Kitani. Wide-baseline multi-camera calibration using person re-identification. In *Conference on Computer Vision and Pattern Recognition (CVPR)*, 2021. 3
- [59] Yufei Xu, Jing Zhang, Qiming Zhang, and Dacheng Tao. Vitpose: Simple vision transformer baselines for human pose estimation. *Advances in Neural Information Processing Systems*, 35:38571–38584, 2022. 2, 3, 5, 6, 9, 1

- [60] Yao Yao, Zixin Luo, Shiwei Li, Tian Fang, and Long Quan. Mvsnet: Depth inference for unstructured multi-view stereo. In *Proceedings of the European conference on computer vision (ECCV)*, 2018. 2
- [61] Vickie Ye, Georgios Pavlakos, Jitendra Malik, and Angjoo Kanazawa. Decoupling human and camera motion from videos in the wild. In *Computer Vision and Pattern Recognition (CVPR)*, 2023. 3, 5, 8, 9, 4
- [62] Kwang Moo Yi, Eduard Trulls, Vincent Lepetit, and Pascal Fua. Lift: Learned invariant feature transform. In *European Conference on Computer Vision (ECCV)*, 2016. 3
- [63] Tao Yu, Zerong Zheng, Kaiwen Guo, and Yebin Liu. Multi-view human body reconstruction from uncalibrated cameras. In *Advances in Neural Information Processing Systems (NeurIPS)*, 2022. 3
- [64] Yuming Yuan, Chun-Hao P. Huang, Donglai Xiang, Yufeng Zhou, Mengcheng Xu, Jingwei Huang, Chenxi Jiang, Tzu-Mao Xu, Deva Ramanan, and Michael J. Black. Human: Multi-modal 4d human dataset for versatile sensing and modeling. In *Proceedings of the IEEE/CVF Conference on Computer Vision and Pattern Recognition (CVPR)*, 2022. 2
- [65] Ye Yuan, Umar Iqbal, Pavlo Molchanov, Kris Kitani, and Jan Kautz. Glamr: Global occlusion-aware human mesh recovery with dynamic cameras. In *Proceedings of the IEEE/CVF conference on computer vision and pattern recognition*, pages 11038–11049, 2022. 4
- [66] Siwei Zhang, Qianli Ma, Yan Zhang, Zhiyin Qian, Taeyun Kwon, Marc Pollefeys, Federica Bogo, and Siyu Tang. Ego-body: Human body shape and motion of interacting people from head-mounted devices. In *European Conference on Computer Vision (ECCV)*, pages 180–200, 2022. 4
- [67] Yizhou Zhao, Hengwei Bian, Kaihua Chen, Pengliang Ji, Liao Qu, Shao-yu Lin, Weichen Yu, Haoran Li, Hao Chen, Jun Shen, et al. Metric from human: Zero-shot monocular metric depth estimation via test-time adaptation. In *The Thirty-eighth Annual Conference on Neural Information Processing Systems*, 2024. 6
- [68] Yizhou Zhao, Tuanfeng Y. Wang, Bhiksha Raj, Min Xu, Jimei Yang, and Chun-Hao P. Huang. Synergistic global-space camera and human reconstruction from videos. 2024. 9, 4
- [69] Shengjie Zhu and Xiaoming Liu. Pmatch: Paired masked image modeling for dense geometric matching. In *Conference on Computer Vision and Pattern Recognition (CVPR)*, 2023. 3
- [70] Yuliang Zou, Jimei Yang, Duygu Ceylan, Jianming Zhang, Federico Perazzi, and Jia-Bin Huang. Reducing footskate in human motion reconstruction with ground contact constraints. In *Proceedings of the IEEE/CVF Winter Conference on Applications of Computer Vision*, 2020. 8

Reconstructing People, Places, and Cameras

Supplementary Material

This is the supplementary material for our main paper “Reconstructing People, Places, and Cameras”. We provide additional qualitative results (Sec. S.1), including in-the-wild examples, a discussion of our approach’s limitations (Sec. S.2), ablation studies on the scale initialization and input views (Sec. S.3), evaluation details (Sec. S.4), implementation details (Sec. S.5), and additional related work (Sec. S.6).

S.1. Additional Qualitative Results

We first present HSfM’s reconstruction results on images captured by two cell phones in Figure S.1. Next, we provide additional qualitative results on EgoExo4D [17] in Figure S.2, showing challenging scenes such as kitchens, humans interacting with objects (e.g., playing the piano), and sports activities like soccer. In Figure S.5, we display further results on EgoHumans [24], demonstrating HSfM reconstructions of multiple people interacting, such as fencing.

S.2. Discussion

Our goal is to study the mutual benefits of jointly reconstructing humans, scenes, and cameras. To this end, we assume that the re-identification of people across camera views is known, because misidentified individuals can introduce spurious effects, disrupting the optimization process. Please note that this limitation also applies to UnCaliPose [57]. To ensure a fair comparison and maintain focus on the core objectives of this study, we rely on ground-truth identities in both our approach and UnCaliPose in the main text.

Since re-identification may not be available at test time and manual identification is cumbersome, we tested the feasibility of automating the re-identification process using the re-identification module of UnCaliPose on the EgoHumans dataset [24]. For re-identification, UnCaliPose solves a constrained clustering optimization problem, assuming a known number of people in the scene and utilizing re-identification features extracted by an off-the-shelf re-identification network [31]. The re-identification process achieves an accuracy of 51.22% on EgoHumans. The main failure mode occurs with individuals wearing uniforms (e.g., tennis sequences: 12.04% accuracy, volleyball sequences: 25.71% accuracy), where appearance features are difficult to distinguish.

These findings indicate that manual re-identification remains necessary for accurate multi-view reconstruction of the world, including humans. Fortunately, modern tools

like LabelMe² simplify this process. Looking ahead, we anticipate that ongoing advancements in large-scale data-model paradigms will significantly improve performance in multi-view re-identification. These advancements may include robust appearance feature matching [34] and the use of geometric similarities, such as human pose and location [16, 37].

While our method achieves good quantitative results, we observe a few failure cases stemming from preprocessing errors in reconstruction and detections. The most common issues arise from erroneous initial camera estimates generated by the scene reconstruction-based SfM[53], particularly in scenes with limited structure, insufficient overlap between images, or large areas affected by radial distortion. In instances where DUST3R[53] fails to detect any cameras, we rely on human-centric camera poses to initialize the optimization. Another source of error involves missing or highly inaccurate keypoint detections, which can occur under conditions of heavy occlusion or poor lighting. In such cases, our method estimates frame-specific cameras solely based on pixel data, without incorporating human constraints.

Despite these occasional errors, we find DUST3R, ViT-Pose [59], and HMR2.0 [16] to exhibit remarkable robustness across a wide range of challenging scenarios.

S.3. Additional Ablation Studies

We analyze the effect of different scale initializations to validate the superiority of the human-centric scaling introduced in Section 4.1 in Table S.1. Without scale initialization ($\alpha = 1.0$), where we directly use the raw DUST3R [53] scene and camera pose outputs as input to our optimization, the W-MPJPE is 11.89m, whereas ours is 1.04m. Additionally, the high metric-scale camera translation errors, such as 6.42m TE, and extremely low RRA values, demonstrate the necessity of proper initialization. This error occurs because the raw camera and scene outputs have a significantly smaller scale than the real world due to their scale normalization during training.

Choosing a large scale value ($\alpha = 100$) generally covers the real-world capture scene sufficiently but does not perform as well as our human-centric scaling approach (W-MPJPE: 1.94m vs. 1.04m). The camera metrics are also worse than ours (e.g., RRA values are 5–7% lower than ours). This implies that, without proper scaling, the optimization is prone to failure due to poor initialization and local minima problems.

²<https://github.com/wkentaro/labelme>



Figure S.1. **Qualitative results *in the wild*.** We show reconstructions on *in-the-wild* images taken with two cell phones and the reconstruction of humans and scene. Our method places people in the world and reconstructs accurate human-scene contact, *e.g.* between the person's right foot and box.

	Human Metrics						Camera Metrics					
	W-MPJPE↓	GA-MPJPE↓	PA-MPJPE↓	TE↓	s-TE↓	AE↓	RRA@10↑	RRA@15↑	RTA@10↑	RTA@15↑	s-RTA@10↑	s-RTA@15↑
S1: $\alpha = 1.0$	11.89	0.85	0.09	6.42	5.50	121.88	0.01	0.01	0.01	0.02	0.01	0.05
S2: $\alpha = 100.0$	1.94	0.22	0.06	2.17	1.11	15.00	0.68	0.82	0.31	0.45	0.68	0.83
S3: HSfM (Ours)	1.04	0.21	0.05	2.09	0.75	9.35	0.72	0.89	0.32	0.46	0.75	0.91
2 Cam. HSfM (init)	3.73	0.42	0.06	1.53	-	9.81	0.41	0.87	0.08	0.12	-	-
2 Cam. HSfM (Ours)	2.63	0.26	0.05	0.39	-	10.37	0.41	0.91	0.48	0.68	-	-
4 Cam. HSfM (init)	4.26	0.51	0.06	2.36	1.14	10.96	0.52	0.79	0.26	0.38	0.49	0.74
4 Cam. HSfM (Ours)	1.15	0.27	0.06	2.00	0.71	8.92	0.68	0.88	0.35	0.50	0.78	0.93
8 Cam. HSfM (init)	5.06	0.53	0.06	2.36	0.96	7.61	0.71	0.87	0.25	0.40	0.65	0.88
8 Cam. HSfM (Ours)	1.00	0.19	0.05	1.97	0.90	7.41	0.76	0.90	0.41	0.54	0.72	0.88

Table S.1. **Ablation on the number of input view cameras.** We evaluate the performance of HSfM by varying the number of input view cameras and assessing human reconstruction and camera pose estimation in the world coordinate frame. The experiments are conducted on EgoHumans, excluding samples without ground truth camera poses for all views in the specified combinations (2, 4, and 8). Compared to the initialization, our joint optimization improves all human pose and camera pose metrics, regardless of the number of input cameras. We do not report the scaled version of camera translation errors for the 2-camera cases, as the predictions become identical to the ground truth camera translations after scale alignment.

One common local minimum observed was humans being placed behind the camera while still reprojecting to the correct pixel locations. To address this, we increased the scale α until all humans were placed in front of all cameras, ensuring positive depth values in all camera coordinate systems. While this initialization produced similar quantitative results in successful cases, it completely failed for 2% of samples, demonstrating that naive initialization approaches are not reliable.

Next, we vary the number of cameras to evaluate the robustness of our method. We tested 2, 4, and 8 input view cameras. As indicated in the table, our joint optimization consistently improves all metrics, regardless of the number of input view cameras. With only 2 cameras, W-MPJPE is 2.63m and GA-MPJPE is 0.26m, indicating accurate human placement in the world. The consistently better camera results compared to the initialization further validate the benefit of incorporating humans into the traditional SfM formulation. The robustness of our method is further demonstrated qualitatively in Figure S.1, where the data is captured by two cameras in in-the-wild scenes.

S.4. Evaluation Details

S.4.1. Evaluation Metrics

In this section, we provide additional details about our human pose and camera metrics.

W-MPJPE describes the mean per-joint position error, measured in the world frame. To bring predicted human meshes into the ground-truth’s world coordinate system, we use an SE(3) rigid alignment from the estimated camera positions to the ground-truth camera positions.

PA-MPJPE describes the Procrustes-aligned variant of MPJPE, which measures position errors after Sim(3) alignment of joints for each human. This metric evaluates local

pose accuracy in a way that is not dependent on camera position estimates or human body scale.

GA-MPJPE evaluates group-aligned joint position errors, computed after Sim(3) alignment for all humans in a scene. This measures people relative to each other, without considering the scene or camera positions.

TE measures the mean Euclidean distance between predicted and ground truth camera positions, after SE(3) alignment. TE evaluates the metric accuracy of camera positions. **s-TE** is the scale-aligned version of TE, where we preprocess positions with Sim(3) instead of SE(3) alignment. This measures scale-invariant errors for estimated cameras.

AE measures the average Angle Error between camera pairs. We compute relative orientations for each pair of cameras in a scene. We then measure the difference between ground-truth and predicted pairwise orientations, convert to degrees, and average.

CCA [27] measures the Camera Center Accuracy, after the SE(3) alignment process used for TE. $CCA@{\tau}$ is the proportion of camera positions with absolute error within $\tau\%$ of the overall scene scale. Following existing work, we compute the scene scale as the furthest distance between a ground-truth camera and the centroid.

s-RTA measures the scale-aligned version of RTA, after the Sim(3) alignment process used for s-TE.

RRA [52] measures the Relative Rotation Accuracy of camera estimates, computed using the same camera pairs as AE. $RRA@{\tau}$ is the proportion of pairwise camera orientations with angular error of τ degrees or lower.

S.4.2. Evaluation Datasets

EgoHumans: In the main text’s tables and Table S.1’s 4 view case, we used the following camera configurations for each sequence:

- For 01_tagging sequences: camera 1, camera 4,

- camera 6, and camera 8.
- For 02_lego sequences: camera 2, camera 3, camera 4, and camera 6.
- For 03_fencing sequences: camera 4, camera 5, camera 10, and camera 13.
- For 04_basketball sequences: camera 1, camera 3, camera 4, and camera 8.
- For 05_volleyball sequences: camera 2, camera 4, camera 8, and camera 11.
- For 06_badminton sequences: camera 1, camera 2, camera 5, and camera 7.
- For 07_tennis sequences: camera 4, camera 9, camera 12, and camera 20.

In Table S.1’s 2 view case, we used the following camera configurations for each sequence:

- For 01_tagging sequences: camera 1 and camera 2.
- For 02_lego sequences: camera 3 and camera 5.
- For 03_fencing sequences: camera 5 and camera 13.
- For 04_basketball sequences: camera 2 and camera 7.
- For 05_volleyball sequences: camera 6 and camera 12.
- For 06_badminton sequences: camera 5 and camera 7.
- For 07_tennis sequences: camera 9 and camera 12.

In Table S.1’s 8 view case, we used the following camera configurations for each sequence:

- For 01_tagging sequences: all 8 available cameras.
- For 02_lego sequences: all 8 available cameras.
- For 03_fencing sequences: camera 1, camera 3, camera 5, camera 7, camera 9, camera 11, camera 13, camera 15.
- For 04_basketball sequences: all 8 available cameras.
- For 05_volleyball sequences: camera 1, camera 3, camera 5, camera 7, camera 9, camera 11, camera 13, camera 15.
- For 06_badminton sequences: camera 1, camera 3, camera 5, camera 7, camera 9, camera 11, camera 13, camera 15.
- For 07_tennis sequences: camera 1, camera 3, camera 5, camera 7, camera 9, camera 11, camera 13, camera 15.

EgoExo4D: Scenes are typically recorded using four to six cameras. For the experiments, we use all available cameras in HSfM and the baselines. We evaluate approximately 200 videos from the validation set, sampling one frame per video. These videos include accurate ground-truth annotations for human poses, locations, and cameras.

S.5. Implementation Details

Given sparse-view images, HSfM jointly estimates SMPL-X [35] parameters for humans, scene pointmaps, and camera poses (rotation and translation), in the world coordinate frame. The SMPL-X parameters for humans are initialized using predictions from HMR2 [16] converted to SMPL-X following the conversion procedure in [33]. Scene pointmaps and camera parameters are initialized with estimates from DUST3R [53]. We use Adam [25] optimizer and set the number of optimization steps proportional to the scene scale with a minimum of 500 steps. This allows sufficient time to accurately determine scene scale and camera poses as well as the locations of people. The learning rate is set to 0.015 with a linear reduction schedule.

S.6. Additional related work

Monocular Human Mesh Reconstruction. Most methods estimate 3D humans in the camera coordinate system for a single person [14, 16, 23, 35] or for multiple people with depth estimation [2, 46, 66]. Recent works jointly estimate human and camera motion in the world coordinate frame [29, 43, 44, 47, 54, 61, 65, 68]. They leverage temporal dynamics from video sequences to improve reconstruction quality over time. While single-view reconstruction methods are valuable for their minimal input requirements, they often suffer from ambiguity, especially due to occlusion. Our approach leverages multi-view data to enhance reconstruction accuracy and integrates scene context, providing a more detailed and reliable reconstruction of multi-person interactions within their environment.

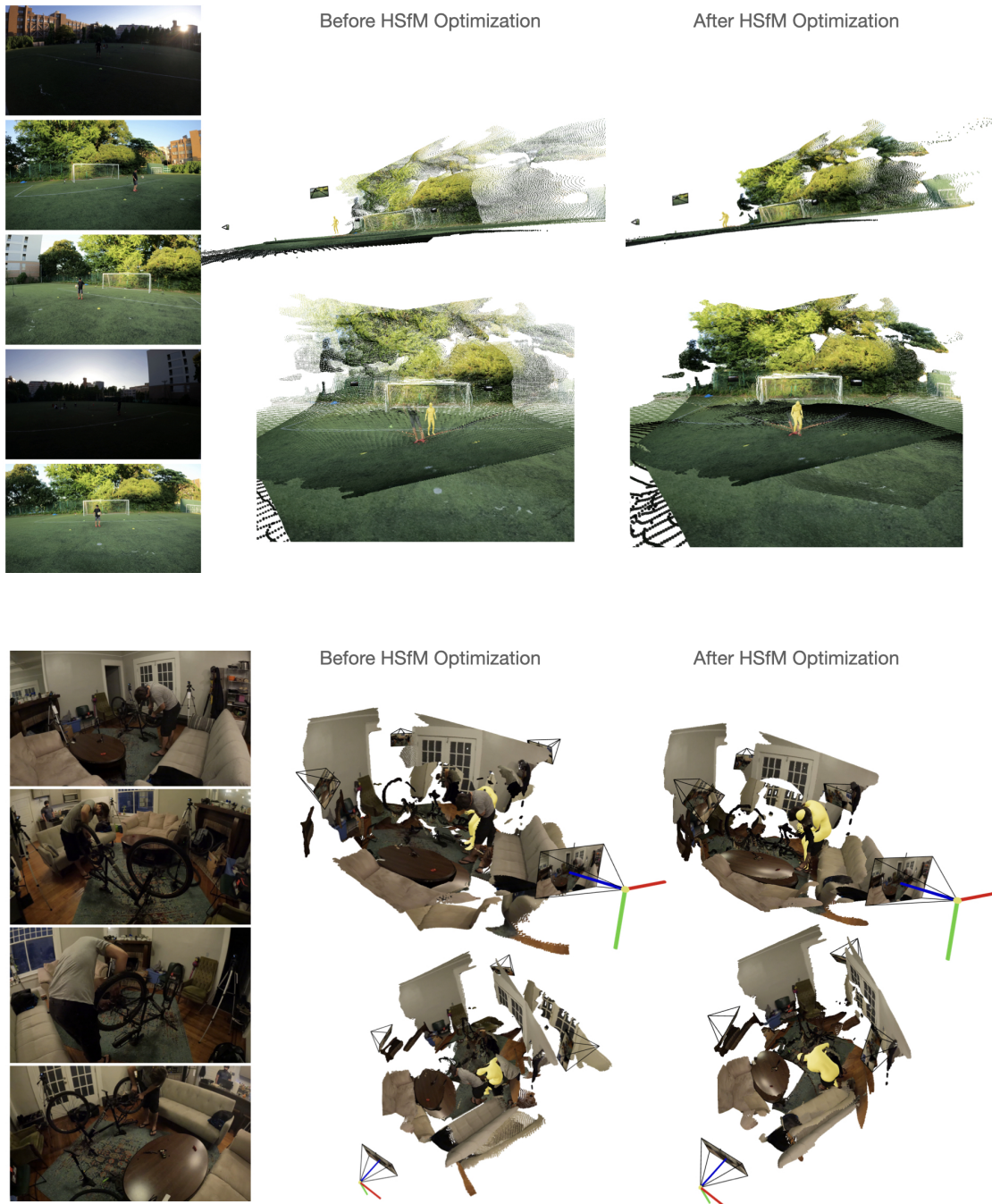


Figure S.2. **Qualitative results.** We show reconstruction on EgoExo4D. On the left, the input images to our method, the scene, humans, and cameras before optimization (HSfM (init.)) in the center, and the reconstruction of our method after joint optimization on the right.

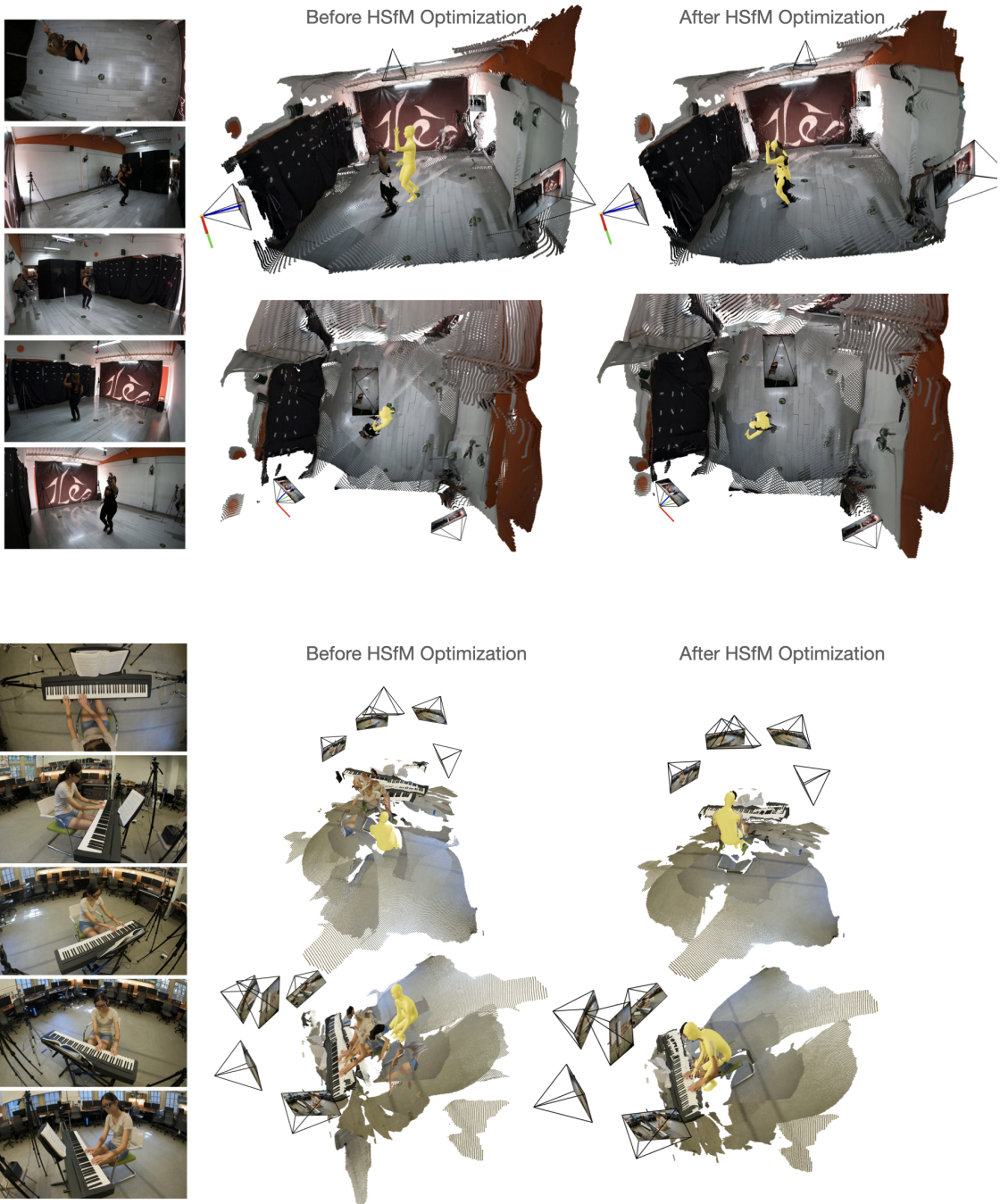


Figure S.3. Continuation of Fig. S.2



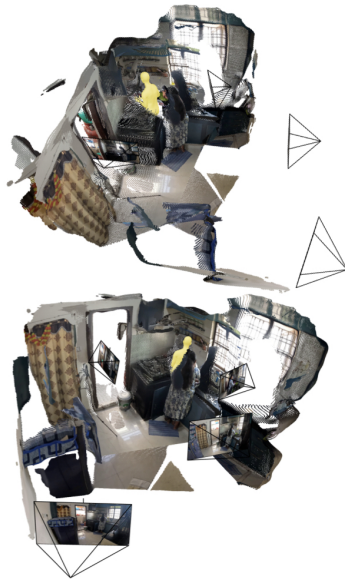
Before HSfM Optimization



After HSfM Optimization



Before HSfM Optimization



After HSfM Optimization

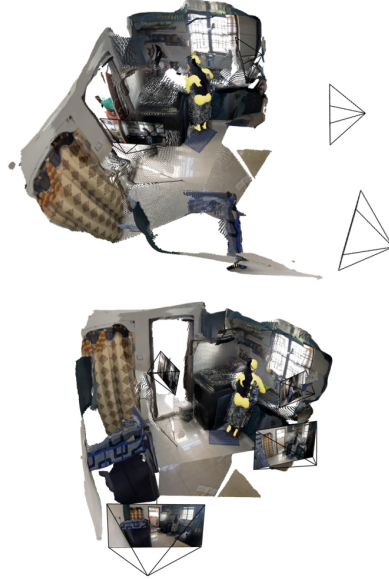


Figure S.4. Continuation of Fig. S.2

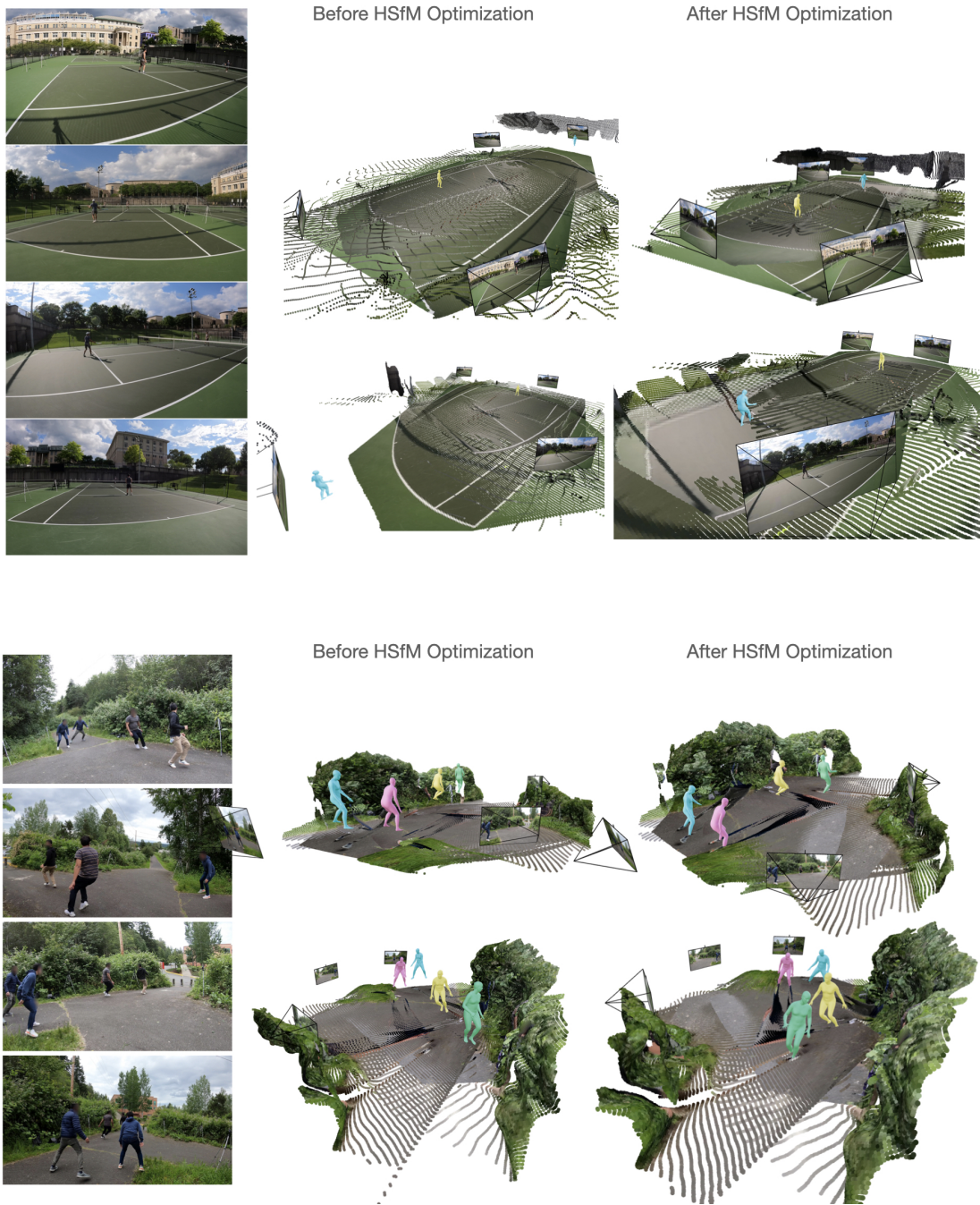


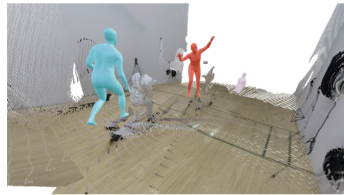
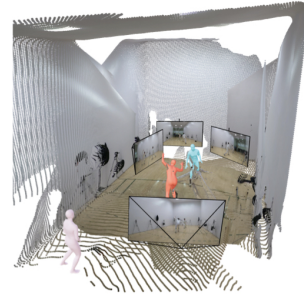
Figure S.5. **Qualitative results.** We show reconstructions on EgoHumans. On the left, the input images to our method, the scene, humans, and cameras before optimization (HSfM (init.)) in the center, and the reconstruction of our method after joint optimization on the right.



Before HSfM Optimization



After HSfM Optimization



Before HSfM Optimization



After HSfM Optimization

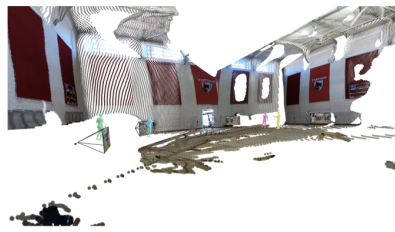
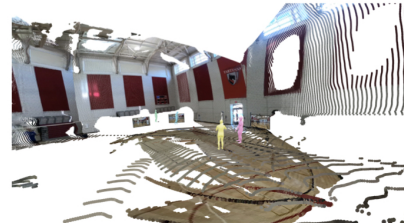


Figure S.6. Continuation of Fig. S.5